An Adaptive Detector and Channel Estimator for Deep Space Optical Communications

R. Mukai, P. Arabshahi, T.-Y. Yan
Jet Propulsion Laboratory
4800 Oak Grove Drive, MS 238–343
Pasadena, CA 91109 USA
[mukai,payman,yan]@jpl.nasa.gov

1 Introduction

Over the past years, NASA and JPL have continuously sought to reduce spacecraft size and mass while increasing its information return capability. Laser communications provide a way of achieving this goal. The highly collimated beam allows for significant reductions in the size and mass of the communications terminal along with reduced power requirements. Optical communications also avoids problems involving radio frequency resource and spectrum allocation, interference, and frequency and bandwidth regulation. Since an increasing number of missions will operate at high downlink data rates, the avoidance of these issues is a significant advantage.

The optical communication system under study at JPL uses pulse-position modulation (PPM) to transmit data. Each PPM symbol consists of 256 signal slots of 20 ns each, and approximately 15 μs of "dead time" (see Fig. 1). The "dead-time" after the 256 slots is present to allow the Q-switched laser sufficient charging time between pulses. Within the slot, there is a small (2 ns) guard time on each side of the 16 ns duration pulse to provide a safety margin against pulse jitter associated with Q-switched lasers [1, 2].

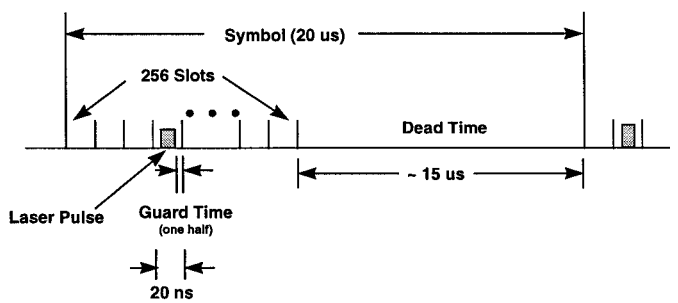

Figure 1: Pulse Position Modulation timing diagram: the slot width T_s is 20 ns; the symbol width T_l is 20 μs; there are $N_s = 256$ slots in a symbol, within which a signal pulse can occur; there are $N_d \approx 750$ dead-time slots in a symbol; and there are about one thousand $(N_s + N_d)$ total slots per symbol.

Space-based optical communication systems are subject to several factors which can impact their performance. Changes in atmospheric conditions on Earth can cause time-smearing, fading, and changes in the received pulse shape [3]. Furthermore, laser communication systems are sensitive to pointing errors, which can cause deep signal fades. As a result, the problem of detecting and acquiring PPM signals under varying channel conditions is a major challenge. If it is known a priori that a PPM symbol does exist, then it is known that the optimal strategy for demodulation is to pick the maximum slot value [4, 5]. However, the problem of initially detecting and acquiring the signal poses a greater challenge since selecting the maximum slot value simply yields a random number if no signal is present.

Hypothesis (Gaussian)	Description	Hypothesis (Exponential)	Description
H_1	$\sigma = 0.1T_s$	H_5	$\tau = \frac{0.5}{\ln(100)}T_s$
H_2	$\sigma = 0.2T_s$	H_6	$\tau = \frac{1.0}{\ln(100)}T_s$
H_3	$\sigma = 0.4T_s$	H_7	$\tau = \frac{2.0}{\ln(100)}T_s$
H_4	$\sigma = 0.6T_s$	H_8	$\tau = \frac{3.0}{\ln(100)}T_s$

Table 1: Hypotheses and pulse shapes corresponding to Figs. 2 and 3.

To address this problem, an adaptive threshold device can be employed to eliminate the "noise-only" case, and assist in the problem of detection and acquisition of the PPM signal. Such a device is a component of an overall "intelligent agent", which, additionally, assists in slot and frame synchronization, control of the phase-locked loop, and determination of channel conditions and characteristics [1, 6].

This signal detection threshold is set based on information received from the intelligent agent, in the form of extracted channel parameters (in turn obtained by analyzing the output of an initial avalanche photodiode detector – APD). We will discuss the design and testing of both the channel parameter identification system, and the adaptive threshold system, in this paper, and illustrate their advantages and performance under simulated channel degradation conditions.

2 Pulse Modeling

It is common for optical pulses to assume Gaussian or exponentially decaying shapes [3, 7] in the time-domain. An ideal Gaussian pulse is described by

$$E[x(t)] = \alpha \frac{n_s}{\sigma\sqrt{2\pi}} \exp\left(-\frac{(t-t_0)^2}{2\sigma^2}\right), \tag{1}$$

where n_s is the average number of signal photons in the signal pulse, σ is the time-domain spread of the pulse, t_0 is the center of the pulse in the time-domain, and α is the multiplicative fade, assumed to be a constant. An ideal exponential pulse with time constant τ is described by

$$E[x(t)] = \frac{\alpha n_s}{\tau} \exp\left(-\frac{t}{\tau}\right) \tag{2}$$

Eight different pulse types and spreads (four Gaussian and four exponential) were tested, as defined in Table 1. In Table 1 hypotheses H_1 and H_5 correspond to "half-width" pulses, which are one-half the normal width. Hypotheses H_2 and H_6 correspond to "full-width" pulses in which 99% of the photons are contained within the 20 ns slot duration (corresponding to 16 samples at our sampling rate). Hypotheses H_3 and H_7 correspond to "double-width" pulses containing 99% of their photons within two PPM slots, and hypotheses H_4 and H_8 correspond to "triple-width" pulses in which 99% of the photons are spread over three slots. In the exponentially decaying case the pulse is defined to start at the beginning of the slot (to catch the largest number of photons in the signal slot), while in the Gaussian case the pulse is centered at the middle of the signal slot (once again to maximize the number of photons in the signal slot itself). Figure 2 illustrates the four Gaussian and exponential pulse types tested.

The attenuation of the signal can be modeled by another multiplicative parameter β, which is a function of α and σ for Gaussian pulses; and α and τ for exponentially decaying pulses.

Once σ, α, and β are known, or adaptively estimated, they can be used in conjunction with receiver operating characteristic (ROC) curves to select the signal detection threshold, λ, in an adaptive manner.

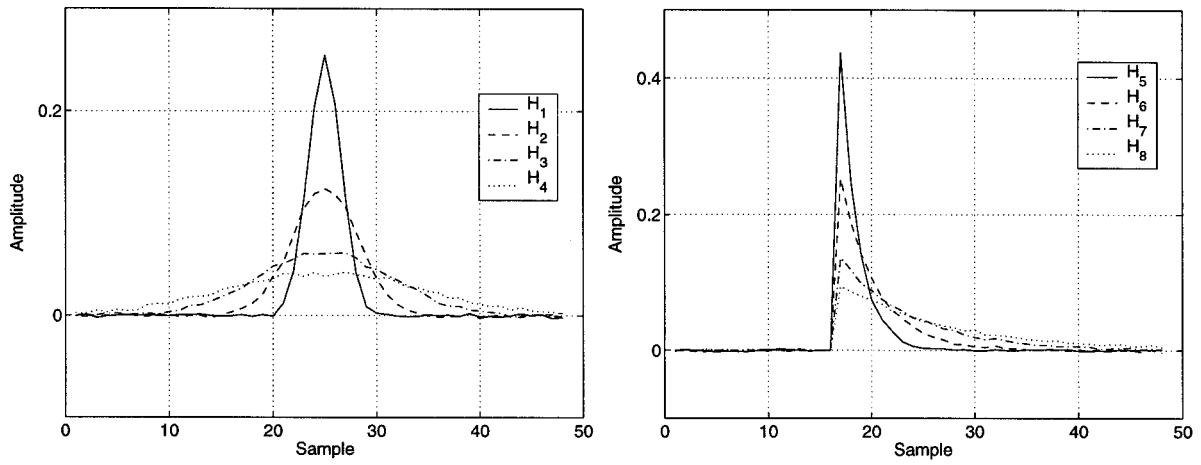

Figure 2: Illustration of Gaussian (left), and exponential (right) pulse shapes used in the simulations. The sampling rate is 800 MHz (16 samples per 20 ns slot). For the Gaussian pulses, three PPM slots (48 samples) are illustrated with the signal slot in the center. The exponential pulses begin at the start of the signal slot in order to maximize photon collection within the signal slot.

2.1 Estimating pulse spread

Neural networks are commonly used to solve problems in pattern recognition [8]. We use a radial basis function network here to recognize pulse shapes, with particular emphasis on determining the pulse spread σ or τ, via the following steps:

1. Noise-only portions of the received PPM symbols (i.e. the "dead-slots") are averaged to compute the ambient background signal. This DC background level is subtracted out, removing daylight effects, and leaving us with only the received signal pulse; thus simplifying the analysis.
2. The vector of pulse samples is normalized to unit L_1 norm. When estimating σ or τ, a great deal of training time can be saved if the neural network is presented with normalized pulse shapes. This improves system reliability as well since the network is less likely to be confused by differences in the pulse caused by fading.
3. The normalized pulse is presented to the neural network for analysis. The network returns a number indicating its estimate of the pulse spread parameter σ for a Gaussian pulse or the time-decay parameter τ for an exponential pulse.

Additional performance improvements can be obtained by using a Reed-Solomon (255,223) code to encode the data in order to detect and remove defective PPM symbols, or possible shot noise events. A total of 255 received symbols are decoded to obtain 223 original data symbols. These are then re-encoded, and the resulting 255 "corrected" symbols are compared to the symbols received from the channel. Any channel symbols differing from the results of re-encoding are considered to be noise events and are ignored. Symbols agreeing with the re-encoded symbols are deemed reliable, and used in the average.

For each symbol to be averaged, three slots (48 samples) consisting of the received PPM signal pulse and its adjacent slots are selected. An average pulse consisting of up to 255 received channel pulses is thus computed. This procedure results in more reliable averaged symbols being presented to the RBF network, allowing very accurate pulse classification.

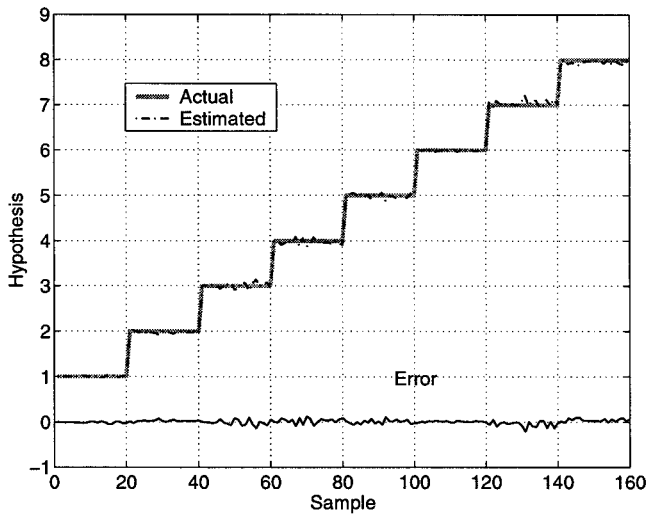

Figure 3: Classification performance of the RBF network without pulse fading. The light gray line denotes actual pulse categories and the darker line denotes the network's classification output. The error is also illustrated.

Figure 3 illustrates the ability of the RBF network to classify pulses based on their pulse spreads. The actual pulse categories and the neural network's classification output are seen to be very close to each other, demonstrating the network's excellent classification accuracy and low error performance.

2.2 Estimating pulse fade α

The fade α of the slot signal is a linear function of the L_1 norm of the pulse calculated during pulse normalization. A family of such linear graphs exists, each with different slopes corresponding to different values of pulse spread. Given a value for the spread (σ or τ), the appropriate curve is selected; its slope computed, and used in conjunction with the correct value for the L_1 norm of the pulse, to estimate α.

Figure 4 illustrates the ability of the system to estimate fades once the pulse spread σ is known. The estimated fades are plotted against actual fades, and it can be seen that the points lie close to the line $y = x$, indicating the accuracy of fade estimation.

2.3 Determining pulse attenuation β

The total multiplicative attenuation β of a Gaussian pulse can be written as

$$\beta = \alpha f(\sigma), \tag{3}$$

where $f(\sigma)$ is the average proportion of "signal photons" contained in the signal slot. This is derived to be

$$f(\sigma) = \int_{-\frac{T_s}{2}}^{\frac{T_s}{2}} \frac{1}{\sigma\sqrt{2\pi}} \exp\left(-\frac{t^2}{2\sigma^2}\right) dt = 1 - 2Q\left(\frac{T_s}{2\sigma}\right), \tag{4}$$

and thus

$$\beta = \alpha\left[1 - 2Q\left(\frac{T_s}{2\sigma}\right)\right], \tag{5}$$

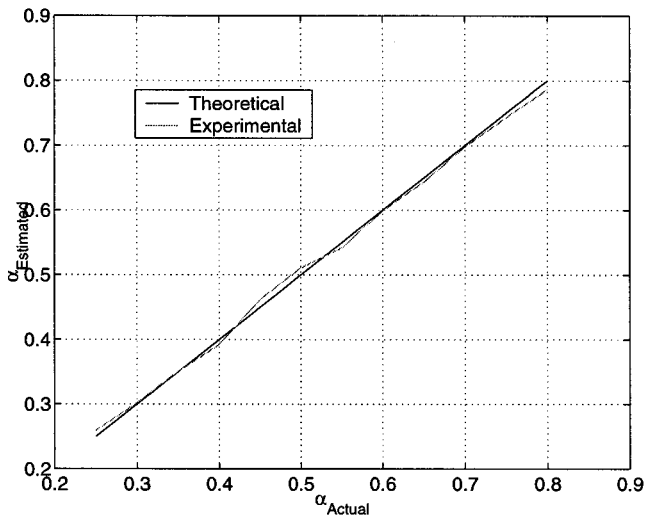

Figure 4: Fade estimation performance for a pulse with $\sigma = 0.2T_s$. Fades ranging from $\alpha = 0.25$ to $\alpha = 0.80$ were estimated under daytime conditions with Gaussian pulses. In this case, a Reed-Solomon error-control code had been used to remove invalid symbols prior to pulse averaging.

as expressed in terms of the commonly used "Q" function in communications. [1]

In the case of an exponential pulse (Eq. (2)), we define the pulse duration as the time T_d which contains, on average, 99% of the photons in the pulse. This yields $\tau = T_d/\ln(100)$ as the pulse's time constant.

Given τ, we compute the average fraction of signal photons in a slot by computing

$$\frac{\int_0^{T_s} \exp(-t/\tau)\,dt}{\int_0^{\infty} \exp(-t/\tau)\,dt} = 1 - \exp(-T_s/\tau) = 1 - (0.01)^{\frac{T_s}{T}} \tag{6}$$

which in turn yields the following for β:

$$\beta = \alpha\left[1 - (0.01)^{\frac{T_s}{T_d}}\right] = \alpha\left(1 - \exp\left(-\frac{T_s}{\tau}\right)\right). \tag{7}$$

3 Pulse Detection

Based on estimates of the above parameters at regular time intervals, we are now interested in determining the receiver operating characteristic (ROC) curves when an adaptive threshold device is in use.

Let P_{FA} be the probability of false alarm. This is the probability that APD noise will exceed the signal detection threshold, thus causing a PPM symbol detection event when no PPM symbol exists. Let P_D be the probability of successful signal detection, which is the probability that if a pulse is present it will be successfully detected. Our hypothesis testing problem can now be formulated as follows: ξ_0 is the hypothesis under which no pulse has been sent, and ξ_1 is the hypothesis under which a pulse has been sent.

Let $p(x|\xi_0)$ denote the probability density function (pdf) of the received slot signal x given hypothesis ξ_0 and $p(x|\xi_1)$ denote the pdf of the received slot signal x given hypothesis ξ_1. Equations (8) and (9) give P_{FA} and P_D in terms of the threshold λ:

$$P_{FA} = P(D_1|\xi_0) = \int_{\lambda}^{\infty} p(x|\xi_0)dx \tag{8}$$

[1] $Q(x) = \sqrt{2\pi}^{(-1)} \int_x^{\infty} \exp(-t^2/2)dt$

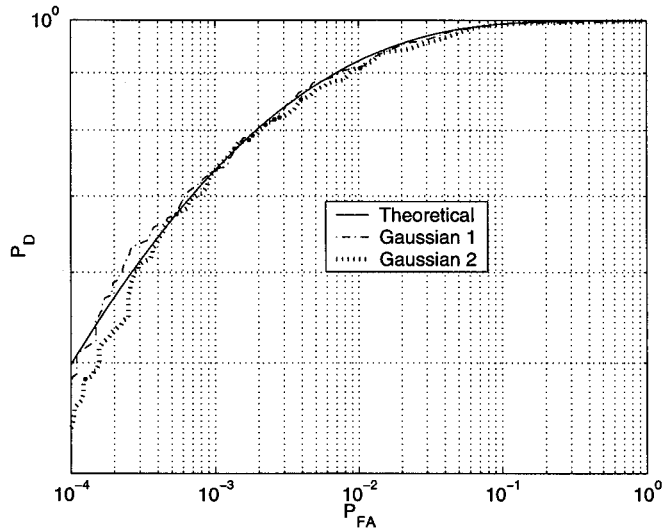

Figure 5: Illustrated here are a "theoretical" ROC curve for $\beta = 0.2900$; and two experimentally obtained ROC curves: "Gaussian 1" for the case where $\sigma = 0.2T_s$ and $\alpha = 0.30$, corresponding to $\beta = 0.2963$, and "Gaussian 2" for the case where $\sigma = 0.6T_s$ and $\alpha = 0.50$, corresponding to $\beta = 0.2977$.

$$P_D = P(D_1|\xi_1) = \int_{\lambda}^{\infty} p(x|\xi_1)dx \tag{9}$$

We then compute the ROC curve for this receiver as a plot of P_D versus P_{FA}. For a given set of channel conditions, P_D will be a function of P_{FA}. The ROC is parameterized by λ, and a given value of λ will yield a point on the ROC. The intelligent agent then uses its knowledge of the channel conditions as determined above, to select the threshold λ.

3.1 The use of β in selecting an ROC

The ROC is itself a function of the overall attenuation β, and it is reasonable to ask whether the use of an overall multiplicative attenuation is justified. This can be an important issue for cases where the time-domain spread of a pulse is large, leading to significant presence of signal photons in slots other than the signal slot (e.g. a Gaussian pulse with spread $\sigma = 0.6T_s$). In fact in such cases, due to the stochastic nature of the received signal, one of the adjoining slots may contribute significantly to P_D.

Experimental results, however, suggest that the ROC typically remains the same for constant β even when there are significant variations in both α and σ for Gaussian pulses (α and τ for exponentially decaying pulses). Figure 5 illustrates this. It can be seen here that in spite of significant differences in pulse shapes the ROC is essentially a function of the total multiplicative attenuation. This in turn justifies the use of β in selection of an ROC curve, followed by selection of an operating point on the ROC, based on user needs.

3.2 Selecting a point on the ROC

The pdf in the noise only case, $p(x|\xi_0)$ (see Eq. (8)), is a function of ambient lighting conditions (average background photons per slot), Gaussian thermal noise in the APD, and the APD's own physical parameters (i.e. APD gain, etc.) Scintillation and fading affect only the signal without affecting either the background photon counts or the thermal noise. This implies that channel conditions primarily affect the ROC and the function of the threshold device through P_D.

If the Neyman-Pearson criterion is used, one could set a threshold using Eq. (8) without considering channel conditions. This may, however, lead to unacceptably low P_D, particularly under conditions of severe scintillation (corresponding to severe time-smearing) and/or severe fading (low values of α). Accordingly, it is often important to take P_D into account, which in turn implies the need to consider channel conditions. We will thus emphasize the selection of a target value of P_D in the experimental results below with the understanding that any receiver must select the threshold λ by considering both P_{FA} and P_D.

4 Experimental Results

We demonstrate the operation of the system below using both Gaussian and exponential pulses.

4.1 Example 1: Gaussian pulse under daytime steady-state conditions

In this first example we focus on a Gaussian pulse received under daytime, steady-state operating conditions. Under these conditions, a Reed-Solomon (255,223) error control code has been used to eliminate "wrong" symbols, leaving only correct pulses to be averaged (assuming no catastrophic decoding errors). The relevant parameters are as follows: fade $\alpha = 0.50$, spread $\sigma = 0.4T_s$, and overall attenuation $\beta = 0.3944$.

Estimation of attenuation β is performed as outlined above. In this example the RBF network output was 2.9780, which is within 1.0% of the correct output of 3.0000 corresponding to hypothesis H_3. The estimated values for the fade and the multiplicative attenuation were $\alpha = 0.4928$ (close to the actual fade $\alpha = 0.5000$) and $\beta = 0.3887$ (close to the theoretical value of $\beta = 0.3944$).

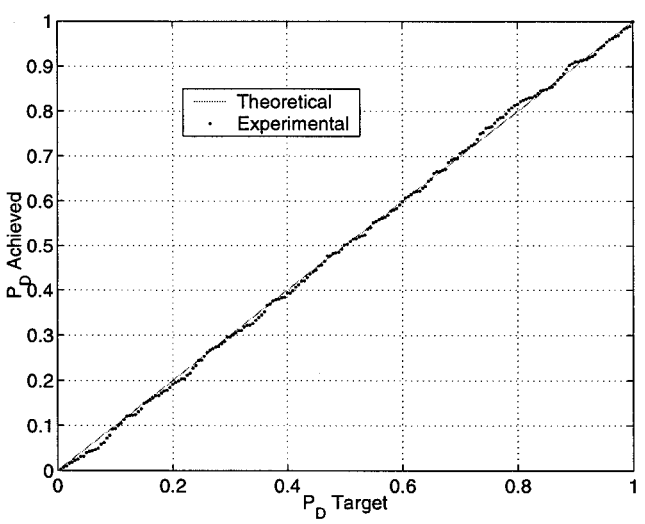

Figure 6: A plot of actual vs. desired probability of signal detection for the case of Gaussian pulses with $\sigma = 0.4T_s$, $\alpha = 0.50$. The closeness of the experimental detection probabilities to the target probabilities illustrates the system's ability to accurately select a signal detection threshold.

At this stage, one could use the simple Neyman-Pearson test to set a threshold, but as explained above, this may not yield an acceptable value of P_D. As stated in Section 3.2, it may be necessary to use knowledge of the exact ROC, which requires knowledge of β, to select the threshold λ. In our simulations, we selected values of P_D ranging from 0.025 to 1.000 in steps of 0.025 by selecting the threshold λ using the parameterized ROC curves. To test the quality of the threshold selection based on β, we can observe the

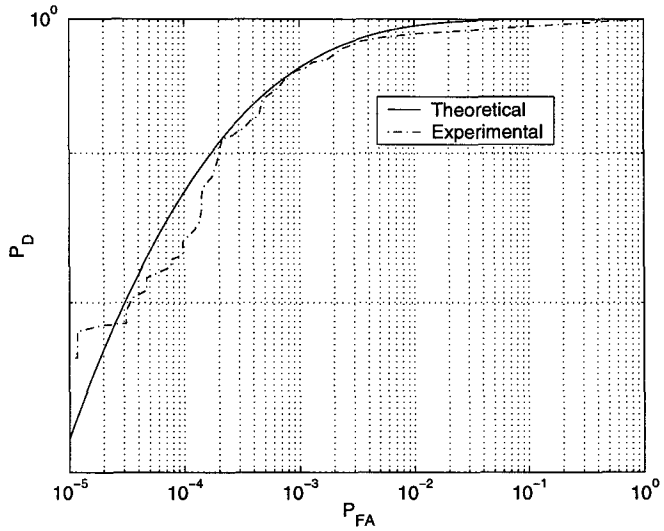

Figure 7: Experimental and actual ROC curves for Gaussian pulses with $\sigma = 0.4T_s$ and $\alpha = 0.50$.

achieved values of P_D plotted against the target P_D. An ideal system should yield a straight line with a slope of 1.0, but a realistic system will yield a noisier line, as illustrated in Fig. 6. The resulting signal detection performance, expressed in terms of P_{FA} and P_D, is shown in Fig. 7.

4.2 Example 2: Exponentially decaying pulse under night acquisition conditions

In the second example, we assume an exponentially decaying pulse received under night conditions and in acquisition mode. This means only ten pulses have been averaged for rapid determination of channel parameters. No error control code is used to remove defective symbols. The relevant parameters are as follows: fade: $\alpha = 0.30$, spread $\tau = \frac{1}{\ln(100)} T_s$, and overall attenuation $\beta = 0.2970$.

Estimation of the attenuation β is done as outlined above. Here the output of the RBF network was 5.8308, which is within 3.0% of the correct output of 6.0000 corresponding to hypothesis H_6. The other parameters are computed to be $\alpha = 0.3057$ (close to the actual fade $\alpha = 0.3000$), and $\beta = 0.3026$ (close to the theoretical value of 0.2970).

Figure 8 shows the achieved P_D vs. target P_D, illustrating the accuracy of the threshold selection process. Figure 9 shows the experimental ROC data versus the theoretical curve. It can be seen that for high P_D, the two curves are quite close.

5 Conclusions

A method for setting PPM pulse detection thresholds using neural-network based estimates of channel parameters has been presented. RBF networks have the ability to accurately determine the shapes of received PPM pulses, permitting an intelligent agent in the optical PPM receiver to determine channel operating conditions and set the appropriate detection threshold for PPM signals. Under a variety of fading and scintillation conditions and under two different families of pulse shapes, the proposed system is able to achieve high accuracy in estimating relevant channel parameters and is also able to accurately select points on the receiver operating curve as needed to achieve a balance between P_{FA} and P_D.

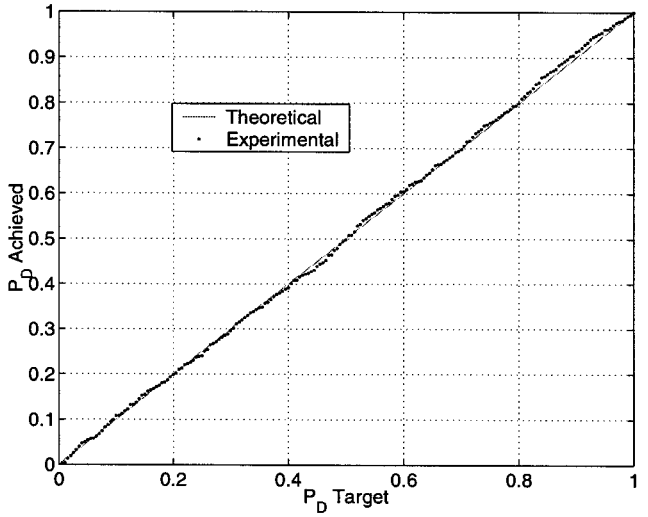

Figure 8: Achieved vs. Target P_D. The threshold selection process yields P_D close to target.

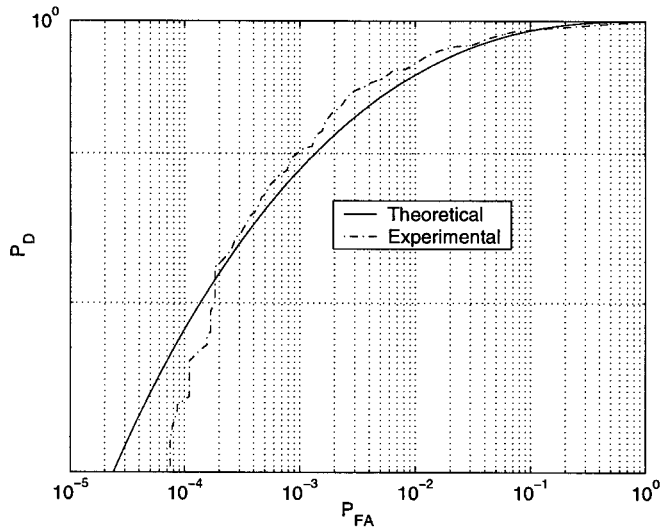

Figure 9: Actual and Theoretical ROC for exponential pulses under acquisition stage conditions.

Future directions include exploration of more sophisticated methods of channel analysis, with an emphasis on improved channel parameter estimation accuracy, and on making better use of channel information. In particular, the system presented here estimates the degree of scintillation (through pulse shape analysis) and the degree of fading as separate numbers. Such information could be used in other ways by an intelligent agent seeking to maintain slot and symbol synchronization in addition to being used for signal detection.

Acknowledgments

The research described in this publication was carried out as part of a task funded by the *Technology and Applications Program* (TAP) at the Jet Propulsion Laboratory, California Institute of Technology, under a contract with the National Aeronautics and Space Administration. The authors wish to express their thanks to Meera Srinivasan and Jon Hamkins for providing the original source code needed for parts of the simulations, and to Victor Vilnrotter for helpful discussions.

References

[1] T.-Y. Yan and C.-C. Chen, "Design and development of a baseline deep space optical PPM transceiver," *Proc. SPIE*, vol. 3615, pp. 154-169, January 1999.

[2] V.A. Vilnrotter, M.K. Simon, and T.-Y. Yan, "The power spectrum of pulse-position modulation with dead time and pulse jitter," *The Telecommunications and Mission Operations Progress Report 42-133*, JPL, Pasadena, CA, May 15, 1998. http://tmo.jpl.nasa.gov/tmo/

[3] Edward A. Bucher, Robert M. Lerner, and Charles W. Niessen, "Some experiments on the propagation of light pulses through Clouds," *Proc. IEEE*, vol. 58, no. 10, pp. 1564-1567, October 1970

[4] M. Srinivasan and V. Vilnrotter, "Symbol-error probabilities for pulse-position modulation signaling with an avalanche photodiode receiver and gaussian thermal noise," *The Telecommunications and Mission Operations Progress Report 42-134*, JPL, Pasadena, CA, August 15, 1998. http://tmo.jpl.nasa.gov/tmo/

[5] M. Srinivasan and V. Vilnrotter, "Performance of the optimum receiver for pulse-position modulation signals with avalanche photodiode statistics," *The Telecommunications and Mission Operations Progress Report 42-133*, JPL, Pasadena, CA, May 15, 1998. http://tmo.jpl.nasa.gov/tmo/

[6] K. Rahnamai, P. Arabshahi, and T.-Y. Yan,"A computationally intelligent fast acquisition algorithm for deep space optical communications," *Proc. Int. Conf. Signal Processing Applications and Technology*, Toronto, Canada, Sept. 1998.

[7] R.M. Gagliardi and S. Karp, *Optical communications*, John Wiley and Sons, 1995.

[8] Simon Haykin, *Neural networks: a comprehensive foundation*, Prentice Hall, 1998.